

The impact of Eastern-Pacific versus Central-Pacific El Niños on the North Equatorial Countercurrent in the Pacific Ocean

Yi-Chia Hsin¹ and Bo Qiu¹

Received 13 July 2012; revised 2 October 2012; accepted 4 October 2012; published 16 November 2012.

[1] Using a three-dimensional ocean reanalysis data product, the influence of two types of the El Niños on the North Equatorial Countercurrent (NECC) across the Pacific basin is examined in this study. Eastern-Pacific El Niños (EP-El Niños) exert a significant impact on the interannual changes of the NECC, whereas Central-Pacific El Niños (CP-El Niños) have little influence. From the developing to mature phase of the EP-El Niños that occurs frequently in the latter half of a calendar year, the NECC tends to intensify and shift southward. While the EP-El Niño-related position changes of the NECC is out of phase with its seasonal position changes, the EP-El Niño-related intensity variability of the NECC is in phase with its seasonal modulation. During both types of El Niños, the El Niño-modulated wind stress curl forcing changes the upper ocean thickness, modifying the NECC intensity and central position. The weaker and shorter fluctuations of wind stress curl forcing during the CP-El Niño events induce irregular and insignificant changes of the NECC.

Citation: Hsin, Y.-C., and B. Qiu (2012), The impact of Eastern-Pacific versus Central-Pacific El Niños on the North Equatorial Countercurrent in the Pacific Ocean, *J. Geophys. Res.*, 117, C11017, doi:10.1029/2012JC008362.

1. Introduction

[2] Flowing to the east along mean latitudes of 5–6°N in the tropical Pacific, the North Equatorial Countercurrent (NECC) is a convergent current of the westward-flowing North Equatorial Current and South Equatorial Current [Reverdin *et al.*, 1994; Johnson *et al.*, 2002; Hsin and Qiu, 2012]. On average, it transports 10–30 Sv (1 Sv $\equiv 10^6 \text{ m}^3 \text{ s}^{-1}$) of the convergent surface warm water from the warm pool in the western Pacific to the east [Wyrski and Kendall, 1967; Philander *et al.*, 1987; Gouriou and Toole, 1993; Donguy and Meyers, 1996; Johnson *et al.*, 2002]. The warm water carried by the NECC has been regarded as one of the factors resulting in the equatorial asymmetry of InterTropical Convergence Zone (ITCZ) in the eastern Pacific [Richards *et al.*, 2009; Masunaga and L'Ecuyer, 2011]. In addition, the NECC intensity and the barotropic shear between the NECC and northern branch of the South Equatorial Current are important in determining the timing of Tropical Instability Wave events in the central Pacific [Philander, 1978; Cox, 1980; Donohue and Wimbush, 1998; Johnson and Proehl, 2004; Lyman *et al.*, 2005]. The NECC strength is also thought of as a critical factor in inducing the tropical sea level changes [Wyrski, 1979] and influencing the

concentration of nutrients in the western Pacific [Christian *et al.*, 2004; Messié and Radenac, 2006].

[3] Using multisatellite surface current data, Hsin and Qiu [2012] have recently examined the seasonal variations of the NECC's center and intensity across the Pacific and explored their forcing mechanisms. In addition to its seasonal modulation, the spectral analysis by Hsin and Qiu [2012] revealed the NECC varied on timescales ranging from days to decades. In the past, interannual variability of the NECC has been proposed to be connected to the El Niño/Southern Oscillation (ENSO) events in the literature [e.g., Wyrski, 1979; Meyers and Donguy, 1984; Kessler and Taft, 1987; Delcroix *et al.*, 1992; Qiu and Joyce, 1992; Johnston and Merrifield, 2000; Johnson *et al.*, 2002; Kessler, 2006]. Most of the studies indicated that the NECC was stronger, or had a larger transport, during the El Niño years (the warm phase of ENSO) [Wyrski, 1979; Meyers and Donguy, 1984; Kessler and Taft, 1987; Taft and Kessler, 1991; Delcroix *et al.*, 1992; Qiu and Joyce, 1992; Johnson *et al.*, 2002]. The NECC was also found to have a more southerly position during the El Niño years [Taft and Kessler, 1991; Johnson *et al.*, 2002]. Johnson *et al.* [2002] suggested that the increase of the NECC transport was $\sim 25\%$ in the El Niño years. By analyzing tidal-gauge records between 160°E and the dateline, Johnston and Merrifield [2000] found that the NECC intensified about 6 months prior to the peak of El Niño (commonly in 1975–1997). However, Johnson and Proehl [2004], from compositing the Acoustic Doppler Current Profiler data between 170 and 110°W during 1991–2001, provided an opposite depiction that the NECC weakened in August–December of the El Niño years. Such a discrepancy could be due to the different data sets and periods used in their respective analyses and it provides one of the

¹Department of Oceanography, University of Hawai'i at Mānoa, Honolulu, Hawai'i, USA.

Corresponding author: Y.-C. Hsin, Department of Oceanography, University of Hawai'i at Mānoa, 1000 Pope Rd., Honolulu, HI 96822, USA. (yichia@hawaii.edu)

This paper is not subject to U.S. copyright.
Published in 2012 by the American Geophysical Union.

motivations to reexamine the NECC variability on the ENSO timescales.

[4] The aim of the present study is to use a fifty-year three-dimensional ocean reanalysis data product to investigate the impact of El Niños on the fluctuations of the NECC across the Pacific basin. Because El Niños can be divided into the conventional and non-conventional types [Larkin and Harrison, 2005; Ashok et al., 2007; Kao and Yu, 2009; Kug et al., 2009; Takahashi et al., 2011], discussions on impact of the two types of El Niños will be the focus of this study. Section 2 introduces the reanalysis data products, the NECC's dynamic properties, and the definitions for the two types of El Niños. Results and discussions are presented in section 3, and summary is made in the final section.

2. Data and Method

2.1. Ocean Reanalysis Data Product

[5] The data used in this study come from the European Centre for Medium-Range Weather Forecasts ocean analysis/reanalysis system (ECMWF ORA-S3) [Balmaseda et al., 2008]. It is obtained from the Asia-Pacific Data-Research Center of the International Pacific Research Center (<http://apdrc.soest.hawaii.edu/>). The reanalyzed temperature, salinity, sea level height and velocity data are available from 1959 to 2009 and they have a horizontal resolution of $1^\circ \times 1^\circ$, 29 levels in the vertical, and a one-month interval. Altimeter-derived sea level anomalies and subsurface temperature and salinity data above 2000 m are assimilated into this reanalysis system. Detailed comparisons of the ORA-S3 system with observational data can be found in Balmaseda et al. [2008]. For the purpose of this study, we follow the definitions adopted in Hsin and Qiu [2012] and calculate the NECC's center and intensity in the period of 1993–2009 from both the ORA-S3 15-m velocity data and the monthly Ocean Surface Current Real-time (OSCAR, <http://www.oscar.noaa.gov/index.html>) data. The correlation coefficients between these two velocity products for both the NECC's center and intensity are about 0.9, indicating the reliability of the ORA-S3 data for describing the variability of the NECC over the longer reanalysis period going back to 1959.

2.2. NECC Center and Intensity

[6] As in Johnson et al. [2002] and Hsin and Qiu [2012], we calculate the NECC's center (Y_{CM}) and intensity (INT) by integrating the positive zonal velocity from surface down to the density level of $26\text{-}\sigma_\theta$ (DR26). DR26 can be regarded as the lower boundary of NECC [Johnson et al., 2002]. The definitions for Y_{CM} and INT are

$$Y_{CM}(x, t) = \frac{\int_{z=DR26}^{z=0} \int_{Y_S}^{Y_N} y \cdot u(x, y, z, t) dy dz}{\int_{z=DR26}^{z=0} \int_{Y_S}^{Y_N} u(x, y, z, t) dy dz} \quad \dots \quad (1)$$

and

$$INT(x, t) = \int_{z=DR26}^{z=0} \int_{\max(Y_{CM}-4^\circ, 2^\circ N)}^{Y_{CM}+4^\circ} u(x, y, z, t) dy dz \quad \dots \quad (2)$$

where x , y , and z are longitude, latitude, and depth; Y_N and Y_S are the northern and southern limits of integration; u is the

zonal velocity and is set to zero for negative u because the NECC is regarded as an eastward flow. The latitudinal limits of integration are the same as those adopted in Hsin and Qiu [2012], i.e., $Y_N = 10^\circ N$ and $Y_S = 2^\circ N$. Hsin and Qiu [2012] suggested that the Y_{CM} and INT values do not change significantly when shifting Y_N northward to $12^\circ N$ or Y_S southward to the equator. In addition, by means of Fast Fourier Transform, Y_{CM} and INT are band-pass filtered within the periods of 500–2500 days in order to highlight their fluctuations on the ENSO timescales.

2.3. Eastern-Pacific versus Central-Pacific Niños

[7] While El Niños have been characterized by anomalous warm temperatures in the eastern Pacific [e.g., Trenberth and Stepaniak, 2001], recent studies have indicated that they can be divided into two types with different formation mechanisms and evolutions [e.g., Larkin and Harrison, 2005; Ashok et al., 2007; Kao and Yu, 2009; Kug et al., 2009; Takahashi et al., 2011]. Different terms have been adopted in naming the two types of El Niños. In this study, we use the “Eastern-Pacific (EP)” and “Central-Pacific (CP)” to distinguish the conventional El Niño with sea surface temperature (SST) warming occurring in the eastern equatorial Pacific from the non-conventional El Niño with SST warming occurring in the central equatorial Pacific Ocean. Note that the CP-El Niños are identical to the events referred to as Modoki El Niños in other papers [e.g., Ashok et al., 2007].

[8] Following the definition in Trenberth [1997], an El Niño is defined as the SST anomalies in the NINO-3.4 area ($5^\circ S$ – $5^\circ N$, 170 – $120^\circ W$) being greater than $0.4^\circ C$ and persisting for at least 6 months. To distinguish the two types of El Niños, we refer to the findings in Kug et al. [2009] and regard an El Niño event as an EP-El Niño if the SST anomalies in the NINO-3 area ($5^\circ S$ – $5^\circ N$, 150 – $90^\circ W$) exceed those in the NINO-4 area ($5^\circ S$ – $5^\circ N$, $160^\circ E$ – $150^\circ W$) over the whole period when the SST anomalies averaged in the NINO-3.4 area exceed $0.4^\circ C$. Conversely, a CP-El Niño is defined when the SST anomalies in the NINO-4 area exceed those in the NINO-3 area. Table 1 classifies El Niños with the peak month when the NINO-3.4 SST has the warmest anomalies (hereafter peak month). Sixteen events occurred during 1960–2009 and, among them, ten are EP-El Niños and six are CP-El Niños. All events began in a year and passed through December to the next year, except for the event of 1993 which spanned a period from March to September within 1993. Most of these El Niño events (75%) reached its peak month between October and December.

[9] In the following sections, composite analyses of flow anomalies, DR26, Y_{CM} , INT, wind vector, and wind stress curl are carried out with the zero-time ($T = 0$) referred to the peak month of each El Niño event. All anomalies are composited without any scaling (i.e., the composite anomalies are not weighted by the strength of El Niños) for EP- and CP- El Niños.

3. Results and Discussions

3.1. Interannual Variability of NECC's Y_{CM} and INT

[10] The normalized, band-pass filtered (500–2500 days), Y_{CM} and INT anomalies (hereafter $Y_{CM}A$ and $INTA$) across the Pacific are shown in Figures 1a and 1c with NINO-3.4

Table 1. Classification of El Niños

Index	Peak Month ^a	Duration (No. of Month)	Type
1	Oct. 1963	Jun. 1963 ~ Feb. 1964 (8)	EP ^b
2	Oct. 1965	May 1965 ~ May 1966 (13)	EP
3	Jan. 1969	Aug. 1968 ~ Jun. 1969 (11)	CP ^c
4	Nov. 1969	Jul. 1969 ~ Mar. 1970 (9)	EP
5	Nov. 1972	May 1972 ~ Mar. 1973 (11)	EP
6	Nov. 1976	Aug. 1976 ~ Apr. 1977 (9)	EP
7	Dec. 1977	Jul. 1977 ~ Feb. 1978 (8)	CP
8	Dec. 1982	Apr. 1982 ~ Jul. 1983 (17)	EP
9	Sep. 1987	Aug. 1986 ~ Feb. 1988 (19)	EP
10	Feb. 1992	Mar. 1991 ~ Jun. 1992 (16)	EP
11	Apr. 1993	Feb. 1993 ~ Sep. 1993 (8)	EP
12	Dec. 1994	Jun. 1994 ~ Apr. 1995 (11)	CP
13	Nov. 1997	Apr. 1997 ~ May 1998 (14)	EP
14	Nov. 2002	Apr. 2002 ~ Mar. 2003 (12)	CP
15	Oct. 2004	Jun. 2004 ~ May 2005 (12)	CP
16	Nov. 2006	Jul. 2006 ~ Feb. 2007 (8)	CP

^aThe month when the NINO-3.4 SST has the warmest value.

^bEastern-Pacific El Niño.

^cCentral-Pacific El Niño.

SST anomaly (SSTA) in Figure 1b. Significant interannual changes in Y_{CM} and INT with variations larger than one standard deviation occur when the NINO-3.4 SSTA peaks positively. This reflects the strong impact of the El Niño events in inducing large changes in the NECC. This El Niño impact is especially significant during EP-El Niños (indicated by yellow bars in Figure 1b). In Figure 2, the zonally

averaged Y_{CMA} and INTA further show that most of the large southward movements ($>$ one standard deviation of $\sim 0.4^\circ$) of the NECC (black line) take place during the El Niño events when the NECC has a larger intensity (red line). Although the La Niña events are not the focus of this paper, we note that the NECC also experiences significant interannual changes associated with negative peaks of NINO-3.4 SSTA.

3.2. Influence of the EP-El Niños

[11] By compositing Y_{CMA} and INTA from the ten EP-El Niño events between 1960 and 2009 (i.e., the ten yellow bars in Figure 2), Figure 3 shows the evolution of Y_{CMA} and INTA from -8 month to 8 month. The southward motion of the NECC ($Y_{CMA} < 0$) starts from the eastern Pacific ($\sim 110^\circ W$) four months prior to the EP-El Niños' peak month and this negative Y_{CMA} moves progressively westward and reaches $\sim 140^\circ E$ nine months later (Figure 3a). The southward movement of Y_{CMA} is estimated at a speed of $\sim 0.5^\circ/day$ to the west, consistent with the westward phase speed of long baroclinic Rossby waves along $5-6^\circ N$ [Meyers, 1979; Kessler, 1990; Chelton *et al.*, 2003] where the mean Y_{CM} is located [Hsin and Qiu, 2012]. This fact indicates that the El Niño-related meridional shift of the NECC is associated with the westward propagating Rossby waves along the mean pathway of NECC. In terms of the composite INTA (Figure 3b), the maximal INTA occurs initially in the central Pacific ($180^\circ-140^\circ W$) half a year

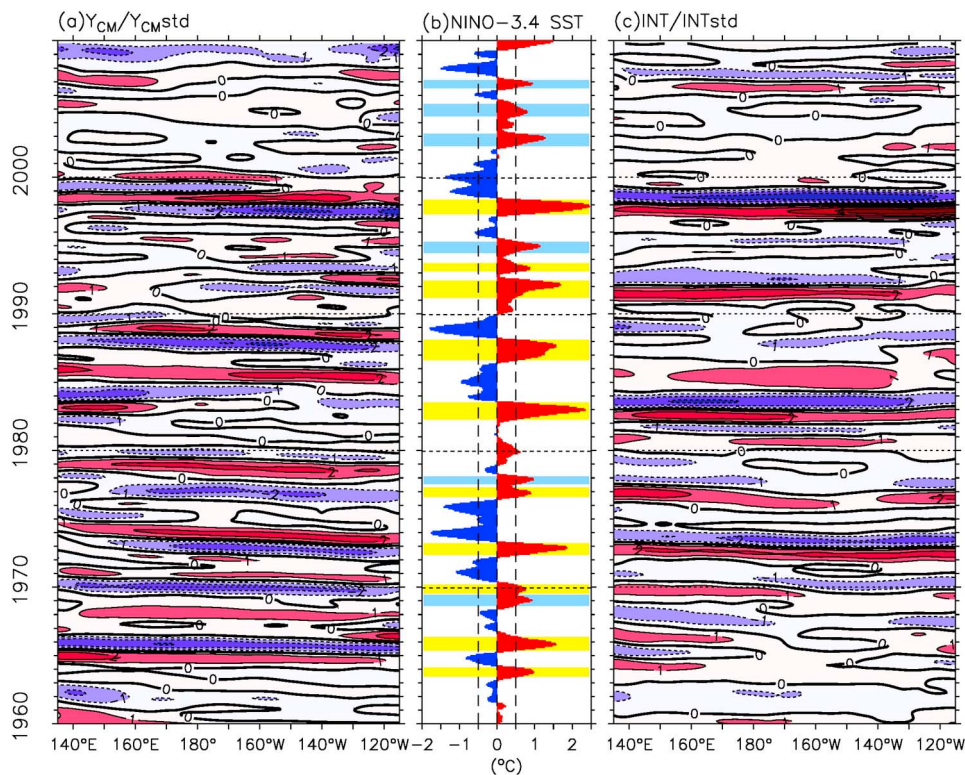


Figure 1. 500–2500-day-bandpassed normalized anomalies of (a) central position (Y_{CM}) and (c) intensity (INT) of the NECC, and (b) NINO-3.4 SST anomaly with EP-El Niño and CP-El Niño in yellow and blue bars, respectively. The normalized anomalies of Y_{CM} and INT are divided by their standard deviation. Contour interval in Figures 1a and 1c is one standard deviation.

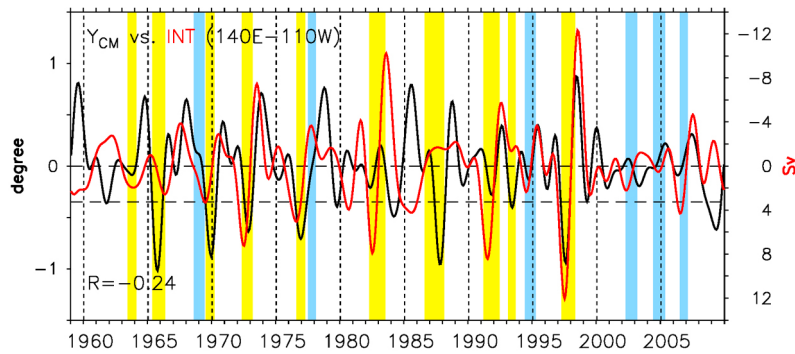


Figure 2. Time series of 500–2500-day-bandpassed anomalies of Y_{CM} (black) and INT (red) averaged over $140^{\circ}E$ – $110^{\circ}W$. Vertical bars in yellow and blue denote EP-El Niño and CP-El Niño, respectively. The reverse scale is used for INT.

before the peak month of EP-El Niños and expands toward both sides of the Pacific. Three (five) months later, the maximal INTA arrives at the eastern (western) Pacific. The propagation speeds of the maximal INTA are estimated at $\sim 0.55^{\circ}/\text{day}$ eastward and $\sim 0.4^{\circ}/\text{day}$ westward.

[12] Composites of anomalies of the 500–2500-day band-pass filtered depth-integral flow (arrow) and DR26 (shading) are shown in Figure 4 to illustrate the evolution of the upper ocean circulation and thermal structures associated with the EP-El Niños. Half a year before the peak month of EP-El Niño, a deepening of DR26 takes place in the east of $\sim 160^{\circ}W$ along the equator, whereas a shoaling of DR26 appears in the western Pacific off the equator (5 – $15^{\circ}N$). Afterwards, DR26 along the equator continues to deepen and shrinks to the east after $T = -4$ month; at the same time, a deepening of DR26 occurs along the east coast of America

north of $5^{\circ}N$ and spreads out to the west. The former reflects the poleward propagation of warm anomalies as coastal Kelvin waves and the latter, the offshore spreading of baroclinic Rossby waves. As to the evolution of DR26 in the western off-equatorial Pacific, it continues to shoal and extend eastward up to $120^{\circ}W$ with a tongue between 5 and $10^{\circ}N$ until $T = 2$ month. Physically, this represents the strengthening of the wind-driven tropical gyre in the western North Pacific Ocean as an EP-El Niño event advances.

[13] The evolution of the NECC is geostrophically related to the changes of DR26, which alter the meridional pressure gradient in the surface layer. Between $5^{\circ}N$ and the equator, an anomalous eastward flow in the east of $\sim 160^{\circ}W$ is intensified by DR26 deepening around the equator from $T = -8$ month to $T = 0$ month while that in the west is intensified by DR26 shoaling north of $5^{\circ}N$ in the western

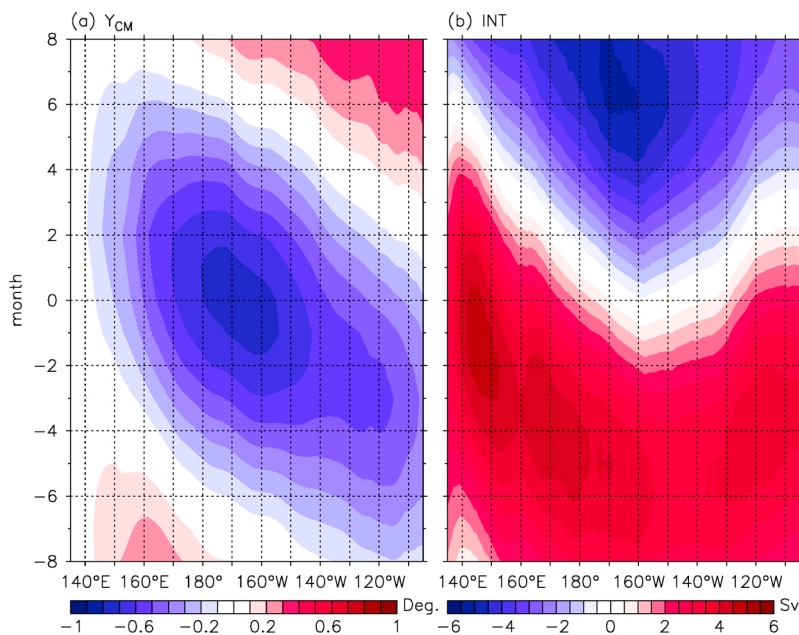


Figure 3. Composites of 500–2500-day-bandpassed anomalies of (a) Y_{CM} and (b) INT from the ten EP-El Niño events showing as the yellow bars in Figure 2. $T = 0$ denotes the month when NINO-3.4 SST has the warmest value for each EP-El Niño event.

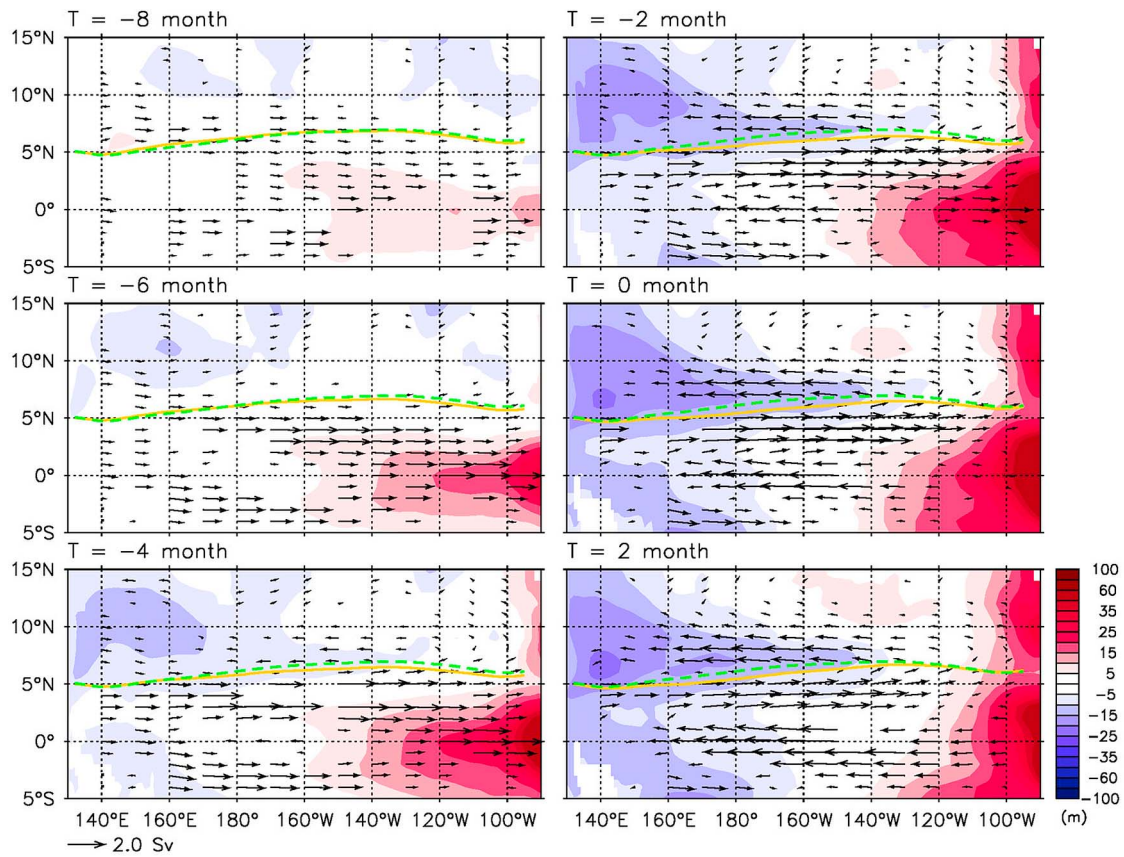


Figure 4. Composites of 500–2500-day-bandpassed anomalies of depth-integral flow (arrow) and depth of the density level of $26\text{-}\sigma_\theta$ (DR26; shading) from the ten EP-El Niño events. $T = 0$ denotes the month when NINO-3.4 SST has the warmest value for each EP-El Niño event. Positive (negative) anomalous DR26 denotes deepening (shoaling). Flow and depth are depicted only when passing the 99% significant level of Student T-test. Yellow line denotes the mean Y_{CM} and green dashed line represents the composite of 500–2500-day-bandpassed Y_{CM} anomaly away from the mean Y_{CM} .

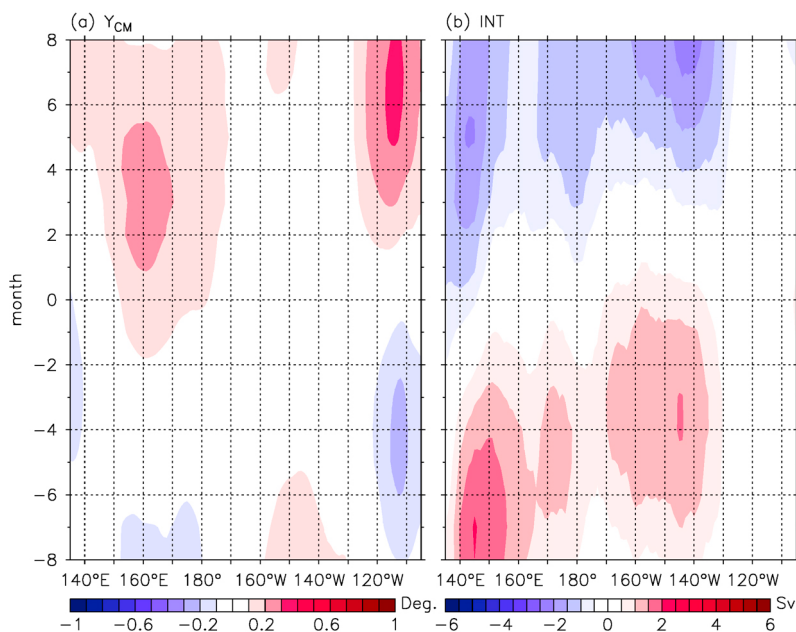


Figure 5. Same as Figure 3 but for the six CP-El Niño events showing as the blue bars in Figure 2.

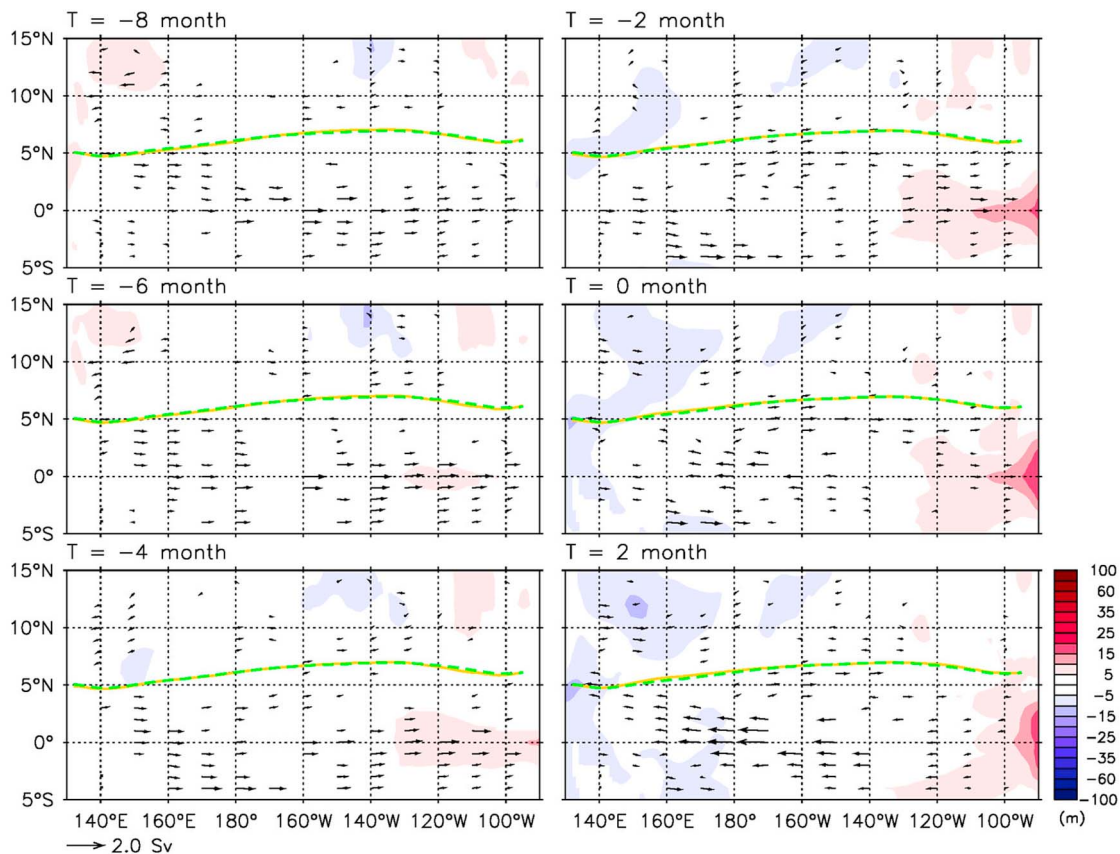


Figure 6. Same as Figure 4 but for the six CP-El Niño events.

Pacific. In 5–10°N, on the other hand, the upper ocean current is changed to a westward anomalous flow with the reinforcement of the westward-extended shoaling of DR26 off the equator. As a result of the anomalous eastward flow south of 5°N and anomalous westward flow north of 5°N, the NECC intensifies with its center shifting to the south during the developing-to-mature phase of the EP-El Niños.

3.3. Influence of the CP-El Niños

[14] With the increasing appearance of CP-El Niños in the 2000s (Table 1 and Figure 1), a question arising naturally is whether the CP-El Niños have a similar impact on the NECC as those of the EP-El Niños. The NECC, as can be seen in Figure 2, does not have a systematic response to the CP-El Niños in terms of its central position and intensity. As shown in Figures 5 and 6, composite analyses based on the six CP-El Niño events marked in Figure 2 by the blue bars reveal relatively weak and irregular anomalies in Y_{CM} , INT, upper-ocean current and DR26 in the tropical Pacific Ocean. While the CP-El Niños have been shown to induce large changes in the global climate, even opposite to those induced by the EP-El Niños [Ashok *et al.*, 2007], their effect upon the NECC in the Pacific Ocean seems to be limited. In spite of this, Y_{CM} east of 120°W shifts to the south prior to the peak month; whereas Y_{CM} west of the dateline changes less before the peak month but moves to the north after the peak month (Figure 5a). In terms of the INT change, in the west of 120°W, it intensifies before the peak month and weakens

after the peak month. Both the intensifying and weakening INT signals tend to propagate eastward from the western Pacific (Figure 5b). Such changes in Y_{CM} and INT are also discernible in the flow pattern in Figure 6. In the eastern Pacific, the southward movement and intensification of the NECC before the peak month is ascribed to the DR26 deepening along the equator although its magnitude is not as strong as that in the EP-El Niño composite.

3.4. Effect of Wind-Forcing

[15] In order to understand the different behaviors of the NECC's interannual variability during the EP- versus CP-Niños, we examine in this subsection the surface wind-forcing based on, again, the composite analyses. During the EP-El Niños, a positive wind stress curl (WSC) anomaly, which induces upward Ekman pumping and shoals the ocean surface layer, exists around 12°N west of the dateline 8 months prior to the peak month, while a positive WSC anomaly forms around 5°N east of ~160°E at $T = -6$ month (Figure 7). Afterwards, the positive WSC anomaly around 12°N weakens, whereas that around 5°N intensifies steadily. The changes of these two positive WSC anomalies result in the evolution of DR26 shoaling shown in Figure 4. Aside from these positive WSC anomalies, negative WSC anomalies prevail north and south of the positive WSC anomalies around 5°N. The northern negative WSC anomaly intensifies from $T = -8$ month to $T = 0$ month whereas the southern one has the opposite evolution. The evolution of these two

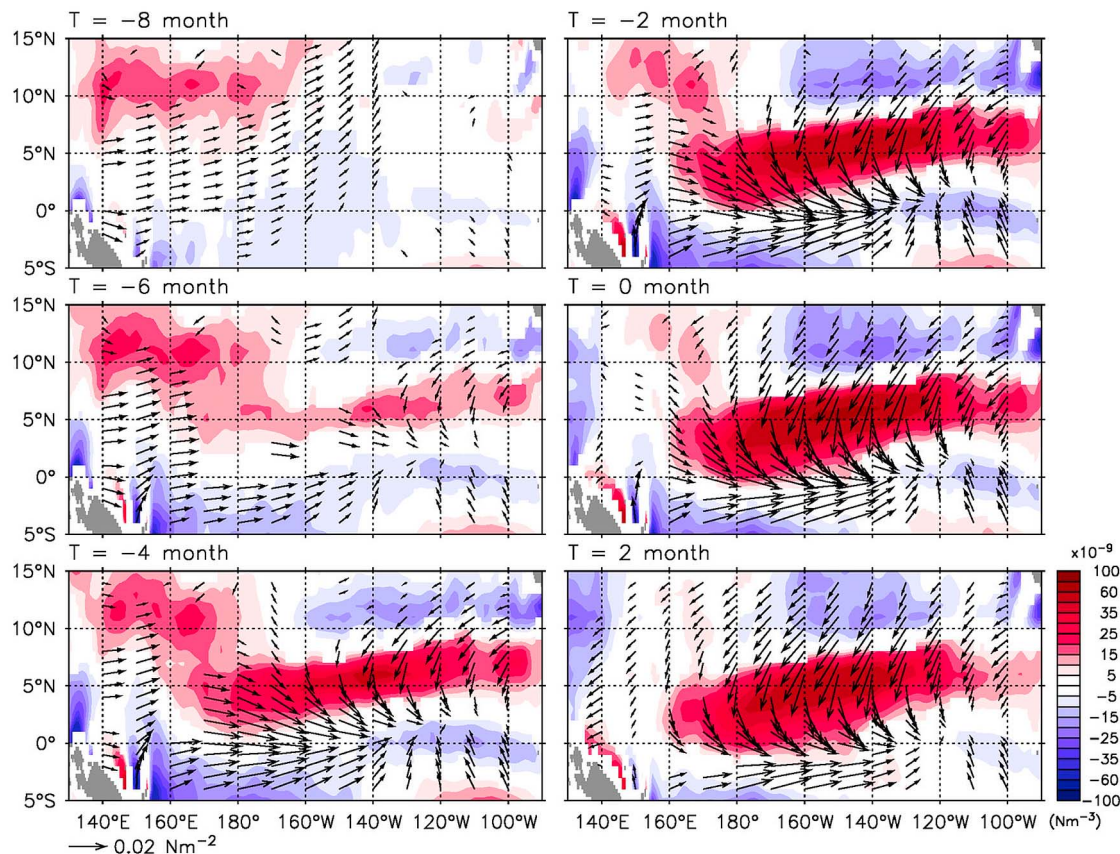


Figure 7. Composites of 500–2500-day-bandpassed anomalies of wind stress vector (arrow) and wind stress curl (shading) from the ten EP-El Niño events. Vector and curl are depicted only when passing the 99% significant level of Student T-test.

negative WSC anomalies corresponds to those of DR26 deepening in Figure 4.

[16] As to the CP-El Niños, their associated fluctuations in wind field are less significant (Figure 8). However, the patterns of WSC anomalies from $T = -2$ month to $T = 2$ month during the CP-El Niños are similar to those during the EP-El Niños with a smaller magnitude. The shorter duration and weaker magnitude of the wind fluctuations during the CP-El Niños are consistent with the results reported in the literature [e.g., Takahashi *et al.*, 2011]. This weaker and shorter wind variation leads to the irregular and feeble responses of anomalous flows and DR26 shown in Figure 6.

[17] It is important to emphasize that the NECC's Y_{CM} and INT signals in each EP-El Niño event can differ (Figure 2). One good example of this is the 1986/1987 El Niño event in which the NECC did not intensify with its southward shift in Y_{CM} . This event started in August 1986, peaked in September 1987, and ended in February 1988 (Table 1); also, it spanned the longest duration of 19 months among the 1960s–2000s El Niño events and is the only event persisting through two winters. Comparing the anomalous flow and DR26 fields during the 1986/1987 El Niño event (Figure 9) to the EP-El Niño composites (Figure 4), the evolution of DR26 during June–December 1987 is in general similar to the composite during $T = -4$ to

2 month, including the westward expansion of DR26 shoaling, the eastward expansion of DR26 deepening north of 5°N , and the westward retreat of DR26 deepening near the equator. However, the anomalous flow in the western Pacific shows a significant difference. From December 1986 to June 1987 (Figures 9b–9e), an anomalous westward flow took place in $0\text{--}5^{\circ}\text{N}$ west of $\sim 160^{\circ}\text{E}$, causing a divergence between 160°E and the dateline and a reduction in the NECC's intensity. Afterwards, this divergence moved westward to $\sim 150^{\circ}\text{E}$ in September 1987 (Figure 9f), the peak month of this event. The difference is attributable to the wind variability in the western Pacific. During March–September 1987 (Figures 10c–10e), an easterly wind prevailed in the western Pacific rather than a westerly wind presented in the composite maps (Figure 7). Meanwhile, in the western Pacific a negative WSC anomaly appeared north of 10°N , resulting in a local deepening of DR26 and a westward anomalous current. This outcome leads to the failed intensification of the zonally averaged NECC during the 1986/1987 EP-El Niño event.

4. Summary

[18] A three-dimensional ocean reanalysis data set is used in this study to investigate the variability of the Pacific NECC on the interannual timescales. The NECC is strongly

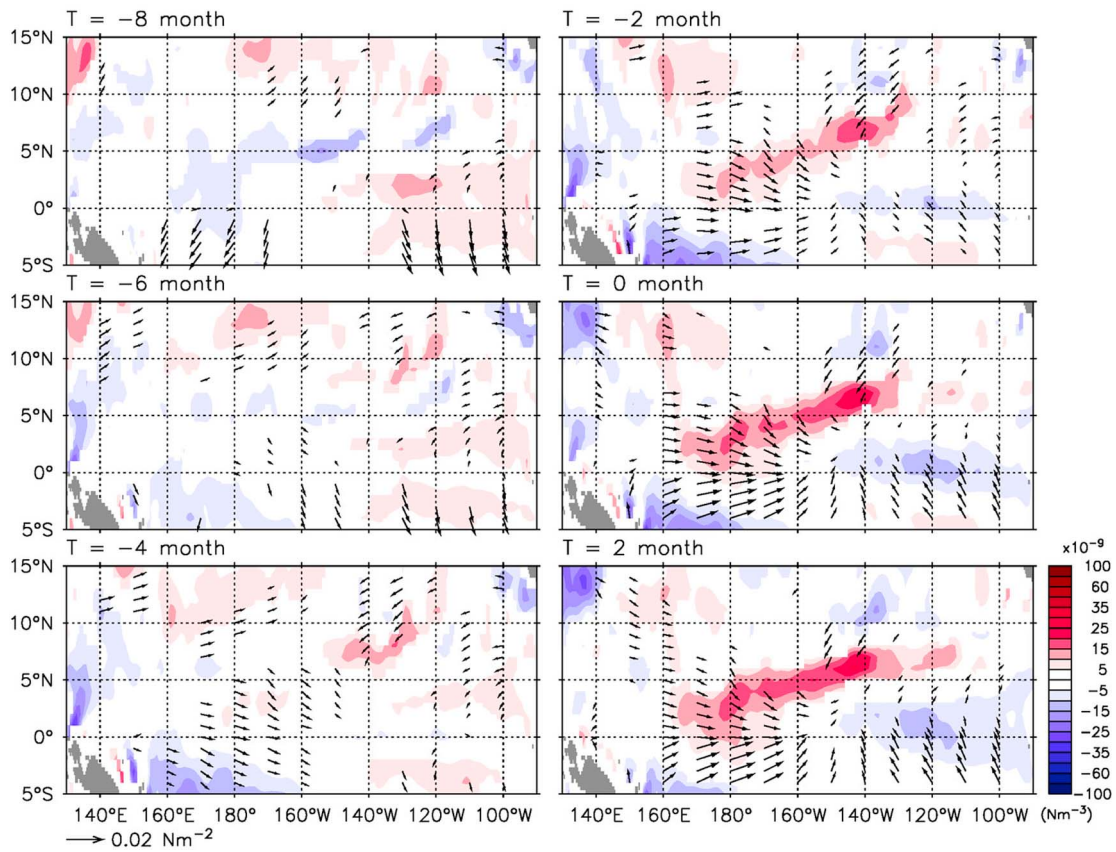


Figure 8. Same as Figure 7 but for the six CP-El Niño events.

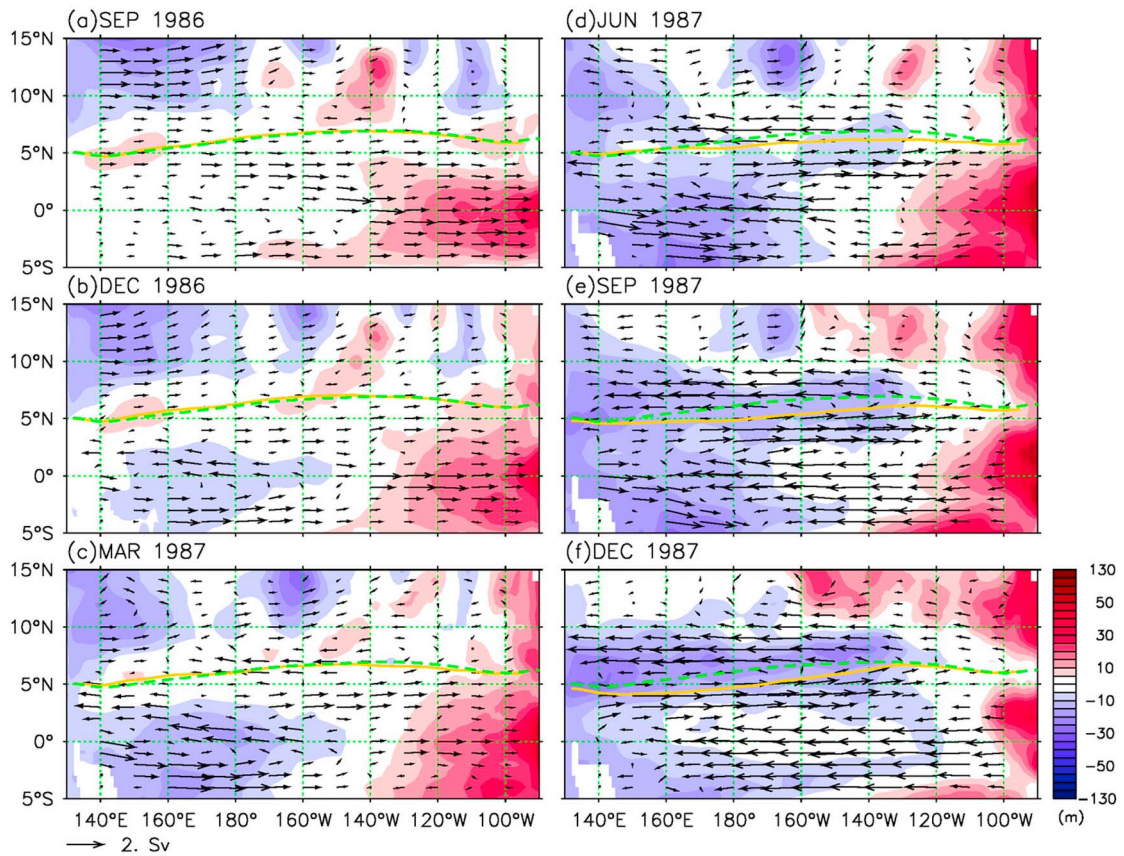


Figure 9. 500–2500-day-bandpassed anomalies of depth-integral flow (arrow) and depth of the density level of $26\text{-}\sigma_\theta$ (DR26; shading) from September 1986 to December 1987. Yellow line denotes the mean Y_{CM} and green dashed line represents the composite of 500–2500-day-bandpassed Y_{CM} anomaly away from the mean Y_{CM} . Anomalies of flow and DR26 are averaged over three months centered at the month labeled above each panel.

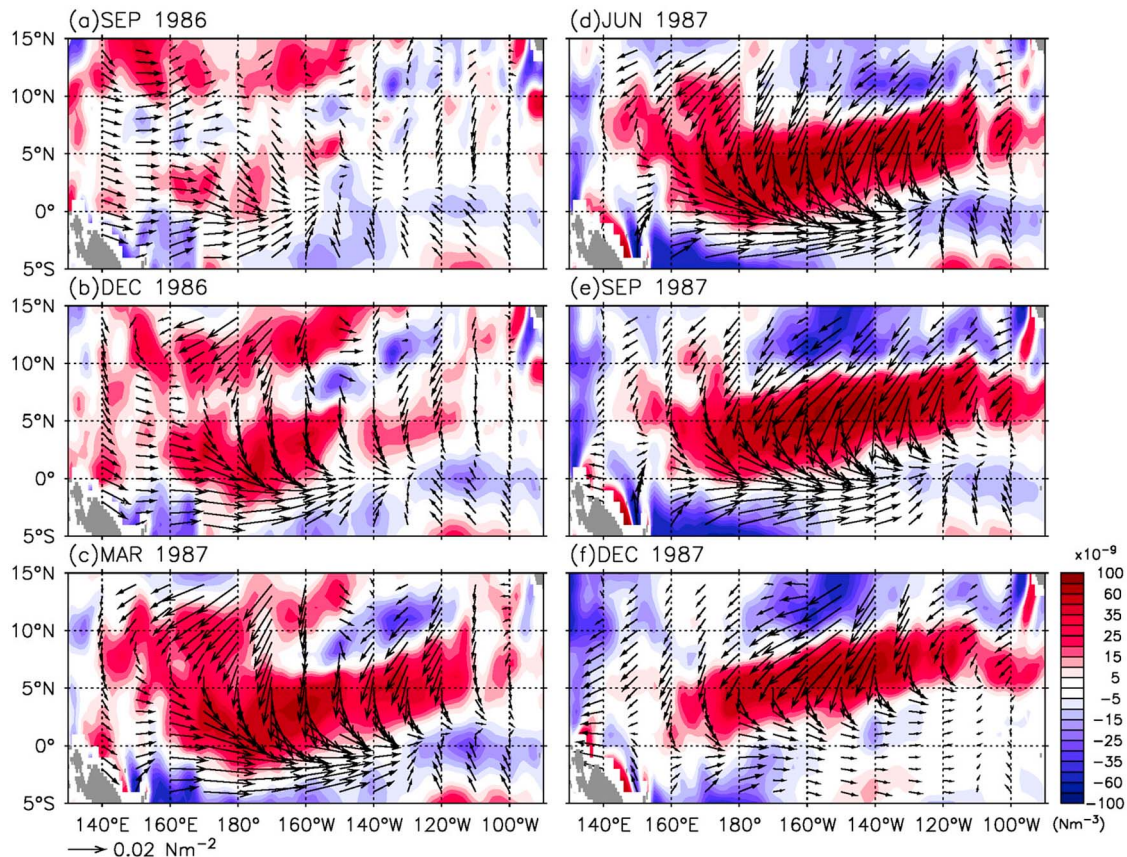


Figure 10. Same as Figure 9 but for 500–2500-day-bandpassed anomalies of wind vector (arrow) and wind stress curl (shading).

influenced by the El Niño events, especially those of the EP-El Niños. Accompanied by the changes in the upper ocean thermal structures, the NECC tends to move equatorward and intensify during the developing to mature phase of the EP-El Niños. This EP-El Niño-induced variability modulates oppositely from the seasonal changes in the NECC's center and intensity. Specifically, on the seasonal timescale, the NECC tends to weaken (strengthen) as it moves equatorward (poleward) in the first (latter) half of a year [Hsin and Qiu, 2012]. In comparison, the NECC variability resulted from the CP-El Niños is relatively small and no systematic response is found in the NECC's central position and intensity.

[19] During the developing to mature phase of both types of the El Niños, a positive wind stress curl prevails zonally around 5°N from the western Pacific to the eastern Pacific with negative wind stress curls existing on the both sides of this positive wind stress curl in the eastern Pacific. In addition, a positive wind stress curl appears north of 5°N in the western Pacific. These positive and negative wind stress curls govern the DR26 evolution around the NECC area, and modulate the upper ocean circulation, including the NECC, on the interannual timescales. However, fluctuations of wind during the CP-El Niños are much weaker and persist for shorter durations than those during the EP-El Niños. As a result, the CP-El Niño-induced flows are chaotic and less significant.

[20] **Acknowledgments.** This research is supported by grant N00014-10-1-0267 of ONR and by contract 1207881 from JPL as part of the NASA Ocean Surface Topography Mission.

References

- Ashok, K., S. K. Behera, S. A. Rao, H. Weng, and T. Yamagata (2007), El Niño Modoki and its possible teleconnection, *J. Geophys. Res.*, *112*, C11007, doi:10.1029/2006JC003798.
- Balmaseda, M. A., A. Vidard, and D. L. T. Anderson (2008), The ECMWF Ocean Analysis System: ORA-S3, *Mon. Weather Rev.*, *136*, 3018–3034, doi:10.1175/2008MWR2433.1.
- Chelton, D. B., M. G. Schlax, J. M. Lyman, and G. C. Johnson (2003), Equatorially trapped Rossby waves in the presence of meridionally sheared baroclinic flow in the Pacific Ocean, *Prog. Oceanogr.*, *56*, 323–380, doi:10.1016/S0079-6611(03)00008-9.
- Christian, J. R., R. Murtugudde, J. Ballabrera-Poy, and C. R. McClain (2004), A ribbon of dark water: Phytoplankton blooms in the meanders of the Pacific North Equatorial Countercurrent, *Deep Sea Res., Part II*, *51*, 209–228, doi:10.1016/j.dsr2.2003.06.002.
- Cox, M. D. (1980), Generation of propagation of 30-day waves in a numerical model of the Pacific, *J. Phys. Oceanogr.*, *10*, 1168–1186, doi:10.1175/1520-0485(1980)010<1168:GAPODW>2.0.CO;2.
- Delcroix, T., G. Eldin, M.-H. Radenac, J. Toole, and E. Firing (1992), Variation of the western equatorial Pacific Ocean, 1986–1988, *J. Geophys. Res.*, *97*(C4), 5423–5445, doi:10.1029/92JC00127.
- Donguy, J.-R., and G. Meyers (1996), Mean annual variation of transport of major currents in the tropical Pacific Ocean, *Deep Sea Res., Part I*, *43*(7), 1105–1122, doi:10.1016/0967-0637(96)00047-7.
- Donohue, K. A., and M. Wimbush (1998), Model results of flow instabilities in the tropical Pacific Ocean, *J. Geophys. Res.*, *103*(C10), 21,401–21,412, doi:10.1029/98JC01912.
- Gouriou, Y., and J. Toole (1993), Mean circulation of the upper layers of the western equatorial Pacific Ocean, *J. Geophys. Res.*, *98*(C12), 22,495–22,520, doi:10.1029/93JC02513.

- Hsin, Y.-C., and B. Qiu (2012), Seasonal fluctuations of the surface North Equatorial Countercurrent (NECC) across the Pacific basin, *J. Geophys. Res.*, *117*, C06001, doi:10.1029/2011JC007794.
- Johnson, E. S., and J. A. Proehl (2004), Tropical instability wave variability in the Pacific and its relation to large-scale currents, *J. Phys. Oceanogr.*, *34*, 2121–2147, doi:10.1175/1520-0485(2004)034<2121:TIWVIT>2.0.CO;2.
- Johnson, G. C., B. M. Sloyan, W. S. Kessler, and K. E. McTaggart (2002), Direct measurements of upper ocean currents and water properties across the tropical Pacific during the 1990s, *Prog. Oceanogr.*, *52*(1), 31–61, doi:10.1016/S0079-6611(02)00021-6.
- Johnston, T. M. S., and M. A. Merrifield (2000), Interannual geostrophic current anomalies in the near-equatorial western Pacific, *J. Phys. Oceanogr.*, *30*, 3–14, doi:10.1175/1520-0485(2000)030<0003:IGCAIT>2.0.CO;2.
- Kao, H.-Y., and J.-Y. Yu (2009), Contrasting Eastern-Pacific and Central-Pacific types of ENSO, *J. Clim.*, *22*(3), 615–632, doi:10.1175/2008JCLI2309.1.
- Kessler, W. S. (1990), Observations of long Rossby waves in the northern tropical Pacific, *J. Geophys. Res.*, *95*(C4), 5183–5217, doi:10.1029/JC095iC04p05183.
- Kessler, W. S. (2006), The circulation of the eastern tropical Pacific: A review, *Prog. Oceanogr.*, *69*, 181–217, doi:10.1016/j.pcean.2006.03.009.
- Kessler, W. S., and B. A. Taft (1987), Dynamic heights and zonal geostrophic transports in the central tropical Pacific during 1979–84, *J. Phys. Oceanogr.*, *17*, 97–122, doi:10.1175/1520-0485(1987)017<0097:DHAZGT>2.0.CO;2.
- Kug, J.-S., F.-F. Jin, and S.-I. An (2009), Two types of El Niño events: Cold tongue El Niño and warm pool El Niño, *J. Clim.*, *22*(6), 1499–1515, doi:10.1175/2008JCLI2624.1.
- Larkin, N. K., and D. E. Harrison (2005), On the definition of El Niño and associated seasonal average U. S. weather anomalies, *Geophys. Res. Lett.*, *32*, L13705, doi:10.1029/2005GL022738.
- Lyman, J. M., D. B. Chelton, R. A. deSzoeke, and R. M. Samelson (2005), Tropical instability waves as a resonance between equatorial Rossby waves, *J. Phys. Oceanogr.*, *35*, 232–254, doi:10.1175/JPO-2668.1.
- Masunaga, H., and T. S. L'Ecuyer (2011), Equatorial asymmetry of the East Pacific ITCZ: Observational constraints on the underlying processes, *J. Clim.*, *24*, 1784–1800, doi:10.1175/2010JCLI3854.1.
- Messié, M., and M.-H. Radenac (2006), Seasonal variability of the surface chlorophyll in the western tropical Pacific from SeaWiFS data, *Deep Sea Res., Part I*, *53*, 1581–1600, doi:10.1016/j.dsr.2006.06.007.
- Meysers, G. (1979), On the annual Rossby wave in the tropical North Pacific Ocean, *J. Phys. Oceanogr.*, *9*, 663–674, doi:10.1175/1520-0485(1979)009<0663:OTARWI>2.0.CO;2.
- Meysers, G., and J. R. Donguy (1984), The North Equatorial Countercurrent and heat storage in the western Pacific Ocean during 1982–83, *Nature*, *312*(5991), 258–260, doi:10.1038/312258a0.
- Philander, S. G. H. (1978), Instabilities of zonal equatorial currents, Part 2, *J. Geophys. Res.*, *83*(C7), 3679–3682, doi:10.1029/JC083iC07p03679.
- Philander, S. G. H., W. J. Hurlin, and A. D. Seigel (1987), Simulation of the seasonal cycle of the tropical Pacific Ocean, *J. Phys. Oceanogr.*, *17*(11), 1986–2002, doi:10.1175/1520-0485(1987)017<1986:SOTSCO>2.0.CO;2.
- Qiu, B., and T. M. Joyce (1992), Interannual variability in the mid- and low-latitude western north Pacific, *J. Phys. Oceanogr.*, *22*, 1062–1079, doi:10.1175/1520-0485(1992)022<1062:IVITMA>2.0.CO;2.
- Reverdin, G., C. Frankignoul, E. Kestenare, and M. J. McPhaden (1994), Seasonal variability in the surface currents of the equatorial Pacific, *J. Geophys. Res.*, *99*(C10), 20,323–20,344, doi:10.1029/94JC01477.
- Richards, K. J., S.-P. Xie, and T. Miyama (2009), Vertical mixing in the ocean and its impact on the coupled ocean-atmosphere system in the eastern tropical Pacific, *J. Clim.*, *22*, 3703–3719, doi:10.1175/2009JCLI2702.1.
- Taft, B. A., and W. S. Kessler (1991), Variations of zonal currents in the central tropical Pacific during 1970 to 1987: Sea level and dynamic height measurements, *J. Geophys. Res.*, *96*(C7), 12,599–12,618, doi:10.1029/91JC00781.
- Takahashi, K., A. Montecinos, K. Goubanova, and B. Dewitte (2011), ENSO regimes: Reinterpreting the canonical and Modoki El Niño, *Geophys. Res. Lett.*, *38*, L10704, doi:10.1029/2011GL047364.
- Trenberth, K. E. (1997), The definition of El Niño, *Bull. Am. Meteorol. Soc.*, *78*, 2771–2777, doi:10.1175/1520-0477(1997)078<2771:TDOENO>2.0.CO;2.
- Trenberth, K. E., and D. P. Stepaniak (2001), Indices of El Niño evolution, *J. Clim.*, *14*(8), 1697–1701, doi:10.1175/1520-0442(2001)014<1697:LIOENO>2.0.CO;2.
- Wyrtki, K. (1979), The response of sea surface topography to the 1976 El Niño, *J. Phys. Oceanogr.*, *9*, 1223–1231, doi:10.1175/1520-0485(1979)009<1223:TROSST>2.0.CO;2.
- Wyrtki, K., and R. Kendall (1967), Transports of the Pacific equatorial countercurrent, *J. Geophys. Res.*, *72*(8), 2073–2076, doi:10.1029/JZ072i008p02073.